Friction **11**(7): 1276–1291 (2023)
https://doi.org/10.1007/s40544-022-0664-z
ISSN 2223-7690
CN 10-1237/TH

RESEARCH ARTICLE

Influence of structural depth of laser-patterned steel surfaces on the solid lubricity of carbon nanoparticle coatings

Timothy MACLUCAS[1,*], Lukas DAUT[1], Philipp GRÜTZMACHER[2], Maria Agustina GUITAR[1], Volker PRESSER[3,4,5], Carsten GACHOT[2,*], Sebastian SUAREZ[1], Frank MÜCKLICH[1]

[1] *Chair of Functional Materials, Saarland University, Saarbrücken 66123, Germany*

[2] *Institute for Engineering Design and Product Development, TU Wien, Wien 1060, Austria*

[3] *INM–Leibniz Institute for New Materials, Saarbrücken 66123, Germany*

[4] *Department of Materials Science & Engineering, Saarland University, Saarbrücken 66123, Germany*

[5] *Saarene-Saarland Center for Energy Materials and Sustainability, Saarbrücken 66123, Germany*

Received: 04 December 2021 / Revised: 07 March 2022 / Accepted: 13 June 2022

Abstract: Carbon nanoparticle coatings on laser-patterned stainless-steel surfaces present a solid lubrication system where the pattern's recessions act as lubricant-retaining reservoirs. This study investigates the influence of the structural depth of line patterns coated with multi-walled carbon nanotubes (CNTs) and carbon onions (COs) on their respective potential to reduce friction and wear. Direct laser interference patterning (DLIP) with a pulse duration of 12 ps is used to create line patterns with three different structural depths at a periodicity of 3.5 μm on AISI 304 steel platelets. Subsequently, electrophoretic deposition (EPD) is applied to form homogeneous carbon nanoparticle coatings on the patterned platelets. Tribological ball-on-disc experiments are conducted on the as-described surfaces with an alumina counter body at a load of 100 mN. The results show that the shallower the coated structure, the lower its coefficient of friction (COF), regardless of the particle type. Thereby, with a minimum of just below 0.20, CNTs reach lower COF values than COs over most of the testing period. The resulting wear tracks are characterized by scanning electron microscopy, transmission electron microscopy, and energy-dispersive X-ray spectroscopy. During friction testing, the CNTs remain in contact, and the immediate proximity, whereas the CO coating is largely removed. Regardless of structural depth, no oxidation occurs on CNT-coated surfaces, whereas minor oxidation is detected on CO-coated wear tracks.

Keywords: solid lubricant coatings; carbon nanotubes; carbon onions; direct laser interference patterning (DLIP) surface structuring; electrophoretic deposition (EPD)

1 Introduction

Friction and wear reduction have been intensively studied for centuries because of their crucial importance in mechanical systems. An effective approach to mitigate friction between two surfaces moving relative to each other is introducing a well-defined surface pattern. It minimizes the real area of contact and possibly entraps abrasive wear particles, thus effectively keeping them out of contact [1–6]. Direct laser interference patterning (DLIP) might be the most versatile and productive among various techniques to create such topographies. During DLIP, multiple high-power laser pulses are brought to interference directly on the substrate's surface, which allows for the creation of periodic surface structures such as line-, cross-, and dimple patterns [7, 8].

Despite environmental concerns and limited applicability in harsh conditions for example, in space applications under vacuum, oil-based lubricants remain

* Corresponding authors: Timothy MACLUCAS, E-mail: timothy.maclucas@uni-saarland.de; Carsten GACHOT, E-mail: carsten.gachot@tuwien.ac.at

the most widely used form of lubrication with few alternatives. However, solid lubricants like graphitic materials and transition metal dichalcogenides have gained increasing attention in recent decades, particularly for extreme environments [9, 10]. Amongst the group of graphitic materials, multi-walled carbon nanotubes (CNTs) and carbon onions (COs), have proven their ability to provide effective solid lubrication either as reinforcement phase in composites [11–18] or as a coating [19–29]. Further studies have shown that CNTs and COs can achieve superlubricity under a specific set of conditions due to the formation of an incommensurate contact [30–33]. Their lubrication ability is attributed to a combination of their mechanical properties based on the sigma bonds formed between sp^2-hybridized carbon atoms and particle morphology [34–37]. While CNTs are cylindrical, COs are spherical, theoretically allowing the particles to rotate and therefore act as a nanoscale roller bearing. This can lead to extremely low coefficients of friction (COF). Hirata et al. [26] conducted ball-on-disc testing with COs spread on a silicon wafer and found a COF value well below 0.1 both in air and vacuum at a normal load of 0.95 N.

On austenitic stainless steel, purely DLIP-processed surfaces wear off rapidly when rubbed against a counter body of similar or higher hardness at sufficiently high loads. On the other hand, carbon nanoparticles are quickly removed from the contact area on a flat sample as they do not form a covalent bond with the chromium oxide layer [22–24]. As shown in a comprehensive review article by Rosenkranz et al. [38], a synergetic approach of textured surfaces combined with solid lubricant coatings like diamond-like carbon (DLC), polytetrafluorethylene (PTFE), and 2-dimensional (2D) layered materials can overcome each approach's limitations. A study conducted by Reinert et al. [23] demonstrated a combination of line-patterned steel surfaces and CNT coatings. Effective solid lubrication was provided over extended periods because the pattern's recessions act as reservoirs from where the lubricant is supplied to the contact area. Neither patterned/uncoated nor unpatterned/CNT-coated samples could provide long-lasting lubrication unless both approaches were combined, in which case a COF of 0.20 was reached and sustained over 10,000 cycles. A ball-on-disc tribometer was used with an alumina ball as a counter body at a load of 100 mN. Surfaces were DLIP-processed with pulses in the nanosecond range resulting in structural depths around 1 μm and subsequently coated with CNTs by electrophoretic deposition (EPD).

In recent years, EPD has been increasingly used to deposit various carbon nanoparticles due to its ability to form homogeneous coatings on geometrically complex substrates while being simple and cost-effective [20, 22–24, 39–41]. Consequently, EPD is a preferred method for manufacturing uniform particle films on steel surfaces.

In a closely related work, Schäfer et al. [22] studied the influence of the structural depth of laser-patterned stainless-steel surfaces, EPD-coated with CNTs. Direct laser writing (DLW) with ultrashort laser pulses in the femtosecond range created cross-patterns with structural depths of 1 and 3 μm. The lubrication performance was measured with a ball-on-disc micro tribometer, working in rotational mode at a normal load of 1 N. Despite having a larger lubricant storage volume, friction experiments with deeper patterns did not lead to an extended lifetime of the lubrication but behaved similarly to the uncoated patterns. This was attributed to the formation of material depositions along the structure's edges, impeding or even blocking the lubricant supply into the contact area.

The present study aims at improving our understanding of such lubrication systems. Stainless steel surfaces are laser-patterned to create line patterns with three different structural depths, thereby changing the slope's angle of the individual line structures. This variation is thought to have a pronounced impact on the laser pattern's ability to supply the contact with lubricious carbon nanoparticles. Surfaces in this work were processed with a pulse length of 12 ps (representing the transition regime between short and ultrashort laser pulses) and generally produced surfaces with slightly different topographies and surface chemistry compared to the nano- or femtosecond regime. Subsequently, EPD was used to coat the as-processed surfaces with CNT and CO films. Platelets

of commercially available AISI 304 austenitic stainless steel were used as substrate material due to the materials' technical relevance and comparability with previous works. The lubrication systems' tribological properties were determined, and the resulting wear tracks were analyzed to determine which structural depth in combination with which carbon nanoparticle coating reduces friction and wear most effectively and permanently.

2 Experimental

2.1 Materials

We used commercially available multiwall CNTs grown by chemical vapor deposition. The material showed an outer diameter of 30–85 nm, a length of 10–15 μm, and was purchased at Graphene Supermarket. COs derived from the annealing of detonation nanodiamonds (NaBond Technologies Co., purity > 98 %, individual particle diameter: 4–8 nm) were used. Annealing was conducted in a vacuum furnace (model: 1100-3580-W1, Thermal Technology Inc.) at a temperature of 1,750 °C for 3 h at a rate of 10 °C/min [42]. As a metal substrate, mirror polished AISI 304 austenitic stainless steel (Brio Kontrollspiegel GmbH) was used in the form of 20 mm × 20 mm platelets with a thickness of 1 mm. Before usage, steel platelets were cleaned thoroughly in acetone and isopropanol baths for 10 min each to remove contamination.

2.2 Pulsed direct laser interference patterning

Line-patterned surfaces were prepared using a Nd:YAG pulsed laser (Edgewave PX-series InnoSlab) integrated into a laser system RDX 500 nano by pulsar photonics. Two equally powerful sub-beams at a pulse duration of 12 ps were used to create line patterns with a periodicity of 3.5 μm. The laser operates with an elliptic laser spot (major axis: 80 μm, minor axis: 57 μm) at a wavelength of 532 nm and the samples were processed at 55% of its maximum power which corresponds to 0.5 W. The step width refers to the shift of the laser spot between each shot, hence a low step width corresponds to a high overlap and, thus, a high fluence. The following step widths were used for structuring: 1/5/10 μm, which translates into a respective fluence of 70/14/7 J/cm^2. Due to oxide formation during laser processing, particularly on surfaces structured at higher fluences, platelets were cleaned after laser processing by ultrasonication first in citric acid, followed by acetone, and finally, isopropanol for 15 min each.

2.3 Surface characterization

To measure the line-patterned steel surfaces' structural depth, the mean height R_C was determined over a sampling length of 259 μm with an Olympus LEXT OLS4100 confocal laser scanning microscope (CLSM) using a 50× objective (NA: 0.95). The equipment operates with a laser wavelength of 405 nm and a vertical and lateral resolution of 10 and 120 nm, respectively. For statistical representation, R_C was measured over 10 different sampling lengths at three different spots on the steel surface.

2.4 Solution preparation and electrophoretic deposition

EPD solutions consisted of 80 mL of isopropanol used as the solvent with 10 mL of triethylamine (TEA). TEA synthesized by ACROS organics with a purity of 99% was used as an additive to support particle deposition. The particle concentration in the solution was 0.1 mg/mL of solvent.

Subsequent particle dispersion was a two-step process. During the first step, the solution was homogenized in a shear mixer (Ultra-Turrax T25, IKA) at 7,000 rpm for 5 min (CO) and 10 min (CNT). Further dispersion was achieved by ultrasonication (Bandelin Sonorex RK514BH) for 10 min (CNT) and 45 min (CO). After the dispersion, two steel platelets were immersed in the solution. Substrate surfaces were arranged in parallel, separated by 1.3 cm, and connected to a DC voltage source. CNTs were deposited at a voltage of 150 V, while for COs, the voltage was set to 300 V. Both particles were processed for 15 min with the deposition occurring on the anode.

2.5 Tribological testing

The friction coefficients' temporal evolution was measured with a ball-on-disc nano-tribometer (CSM

Instruments) in linear-reciprocating mode transversal to the line-pattern. The stroke length was set to 0.6 mm and the velocity to 1 mm/s. A normal load of 100 mN was chosen, corresponding to a Hertzian contact pressure of 360 MPa. Alumina balls (grade 28, Anton Paar GmbH) measuring 6 mm in diameter, with a surface roughness of R_Q = 55.5 ± 12.8 nm were used as a counter body. 10,000 measurement cycles were conducted at room temperature and a constant relative humidity of 4%. This humidity level was explicitly chosen to exclude graphitic lubrication, which is enhanced by the presence of water vapor as it significantly facilitates interlamellar shearing of individual graphite or even graphene crystals [9]. For statistical representation, each sample was tested three times. The resulting raw data were slightly smoothed (Savitzky-Golay filter, 50 p) before being used to plot the COF development graphs.

2.6 Chemical and microstructural characterization

Micrographs of the coatings, cross-sections, and wear tracks were made with a Helios NanoLab 600 dual beam workstation (scanning electron microscope (SEM)/focussed ion beam (FIB)) by FEI. Subsequently, the wear tracks were characterized by energy-dispersive X-ray spectroscopy (EDS) with an EDAX detector. While EDS was performed at an acceleration voltage of 15 kV and a current of 11 nA, SEM micrographs were taken at 5 kV and 1.4 nA. Transmission electron microscopy (TEM) samples were extracted from the center of the wear track in the direction parallel to the sliding motion. The preparation was done using a focussed ion beam (FIB-Helios Nanolab 600-FEI Company) as detailed in [43]. A JEOL JEM 2010F was utilized for TEM at an acceleration voltage of 200 kV.

3 Results

3.1 Surface topography

To visualize the profiles of the patterns created by DLIP-processing, CLSM was used for coarse-scale 3D mapping. The maps shown in Fig. 1 span an area of approximately 170 µm × 170 µm and demonstrate pattern uniformity regardless of fluence and, thus, structural depth. In addition to that, FIB cross-sections were made and imaged by SEM. The FIB-cross sections depicted in Fig. 2 (CNT-coated) and Fig. 3 (CO-coated) show the topographies of the laser-patterned and coated samples processed at different structural depths. Pronounced curtaining is observable in the scanning electron micrographs of both coatings, particularly in the case of the COs and can be attributed to the high porosity of the coatings as it prevents the formation of a coherent protective platinum deposition. This porosity is a consequence of the formation of large and poorly interconnected agglomerates. Compared to CNTs, COs form smaller agglomerates as a result of which more homogeneous coatings are formed. CNTs are cylindrical with a high aspect ratio and a strong tendency to entangle. Convex flanks characterize both the shallow (Figs. 2, 3(a), and 3(d)) and the intermediate structures (Figs. 2, 3(b), and 3(e)), whereas the deeper structures (Figs. 2, 3(c), and 3(f)) exhibit a concave profile as well as higher burrs on each side of the line-like structure.

The three different structural depths were achieved by varying the laser spot's step width along the line-like structure. Laser processing at shorter step widths means more significant spot overlap and higher fluences, resulting in deeper structures with steeper flanks. This is confirmed by the results listed in Table 1.

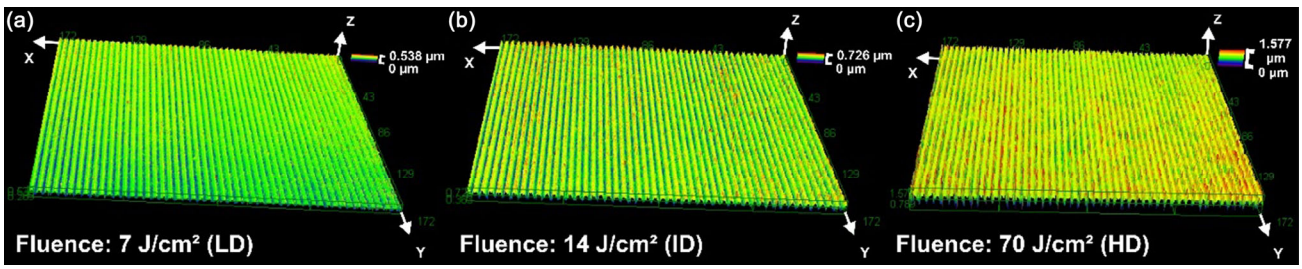

Fig. 1 Coarse-scale 3D maps of the patterned surfaces processed with fluences of (a) 7, (b) 14, and (c) 70 J/cm^2 resulting in different structural depths (low depth (LD), intermediate depth (ID), and high depth (HD), respectively). The maps were made using CLSM and display an area of approximately 170 µm × 170 µm (zoom: 1.1, *z*-factor: 9.1).

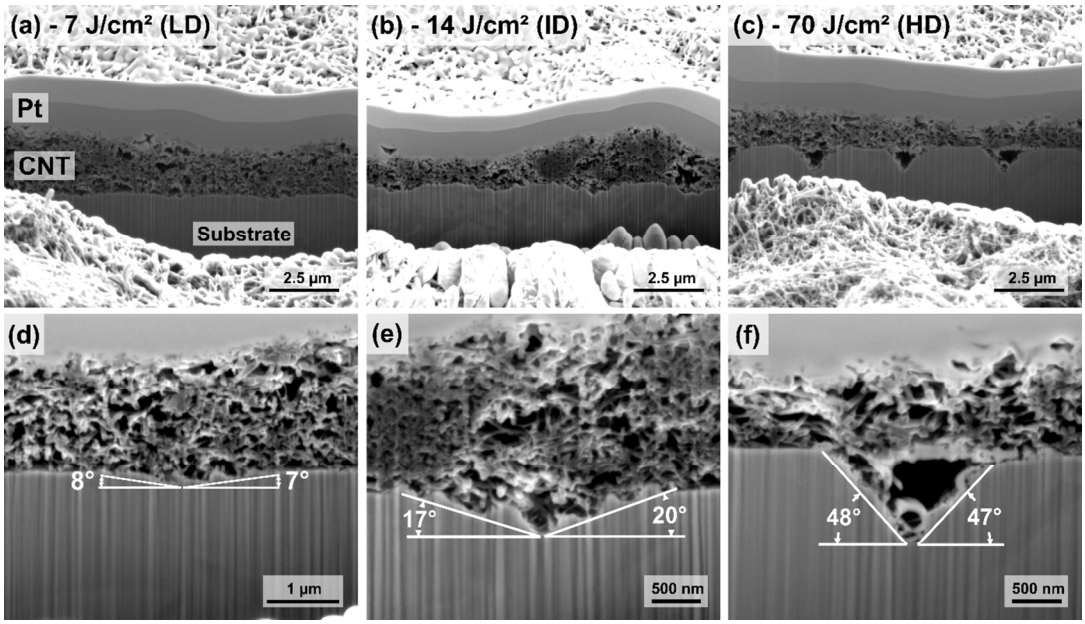

Fig. 2 FIB cross-sections of CNT-coated picosecond-laser processed steel surfaces at fluences of (a, d) 7, (b, e) 14, and (c, f) 70 J/cm^2 resulting in structural depths of 0.24, 0.36, and 0.77 µm, respectively.

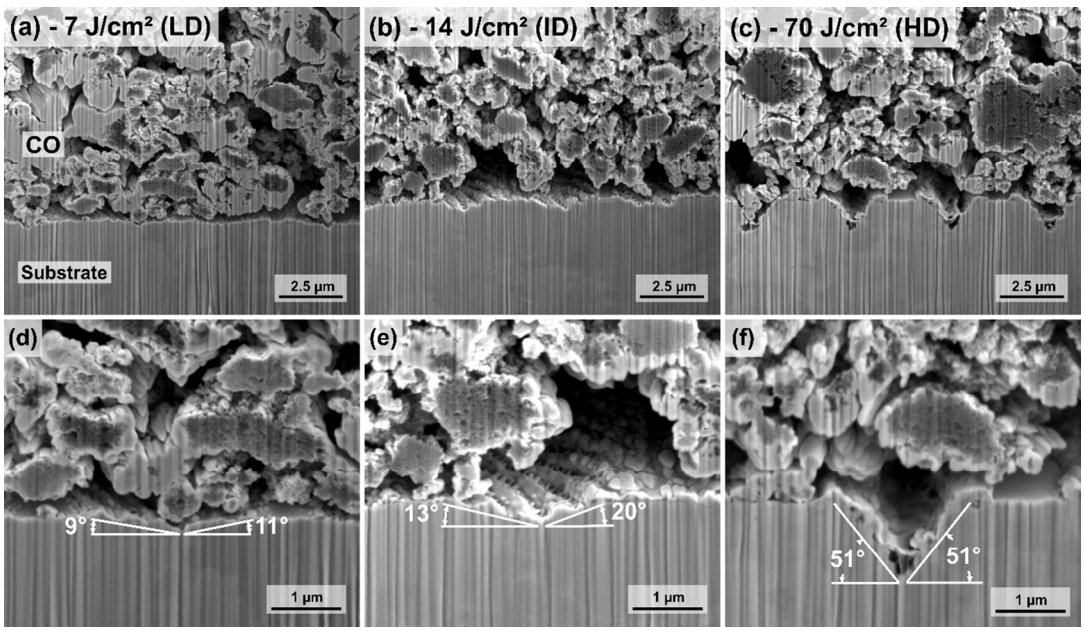

Fig. 3 FIB cross-sections of CO-coated picosecond-laser processed steel surfaces at fluences of (a, d) 7, (b, e) 14, and (c, f) 70 J/cm^2 resulting in structural depths of 0.20, 0.39, and 0.78 µm, respectively.

Table 1 Mean height R_C and slope angles of the line-patterned steel surfaces processed at different fluences.

Sample acronym	Fluence (J/cm^2)	Mean height R_C (µm)		Slope angles (°)	
		CNT-coated	OLC-coated	CNT-coated	OLC-coated
LD	7	0.237 ± 0.006	0.196 ± 0.002	9.7 ± 1.6	10.0 ± 3.0
ID	14	0.355 ± 0.003	0.389 ± 0.007	19.1 ± 3.4	16.3 ± 3.8
HD	70	0.770 ± 0.007	0.779 ± 0.020	47.0 ± 4.8	48.6 ± 2.9

The standard deviation of the structural depths is very low and lies between 0.8% and 2.6% for both CNT-coated and CO-coated surfaces. Therefore, the patterns can be described as highly homogeneous throughout all measured surfaces. Comparing the absolute depths of both substrates, patterned with the same fluence, shows that the shallow patterns are comparable. In contrast, the intermediate and deep patterns are close to identical, demonstrating the high reproducibility of the DLIP technique. For the smallest structural depth, produced with the longest step width, the substrate's initial state (e.g., roughness, absorptivity) will have a more significant effect on the result, thus slightly affecting the reproducibility.

Differing structural depths result in flanks with different slopes. Both features of the respective structures are listed in Table 1. The values obtained for CNT-coated and CO-coated structures do not deviate in any statistically significant way and are highly comparable.

3.2 Friction behavior

Figure 4 shows the temporal evolution of the COF. In both friction tests, Ref represents a non-patterned, mirror-polished stainless-steel substrate used as a reference. When rubbing against the aluminum oxide counter body, the COF of Ref rises sharply and reaches an early steady-state at 200–250 cycles after which, it oscillates between 0.7 and 0.8. According to Blau et al. [44], the tribological behavior is characteristic of dry metal-metal contact, where the metals' surfaces are either contaminated (e.g., hydrocarbons, adsorbed water) or covered by oxides. Furthermore, the obtained values lie within the range of what we have measured under identical conditions in previous works [20, 22–24].

The patterned and uncoated samples show similar tribological behavior as the reference, regardless of their respective structural depth. The COF of the LD and ID samples increase immediately and sharply, concurrent with the reference. In contrast, the increase in COF for the HD sample is slightly delayed. HD's asperities are significantly deeper; therefore, more material needs to be abraded until conformal contact is achieved. Thus, the real area of contact between surface and counter body remains reduced for more extended periods. The running-in behavior of LD and HD can be classified as type *a* according to Blau [44], while ID shows a clear type *b*. Both behaviors are typical for unlubricated metal contacts. The steady-state COF of all patterned surfaces without coating is comparable and oscillates around 0.7.

Coating the patterned surfaces with carbon nanoparticles results in an entirely different frictional behaviour. Generally, the samples combining both laser-patterning and CO coatings demonstrate a small COF peak at the very beginning of the test, which could be associated with a re-arrangement of the particles in the contact region until conformity is achieved. The initial peak is followed by a friction reduction down to COF values of 0.25–0.35. This represents a significant improvement compared to the reference or the merely laser-patterned samples, which can be ascribed to the lubricity of the COs

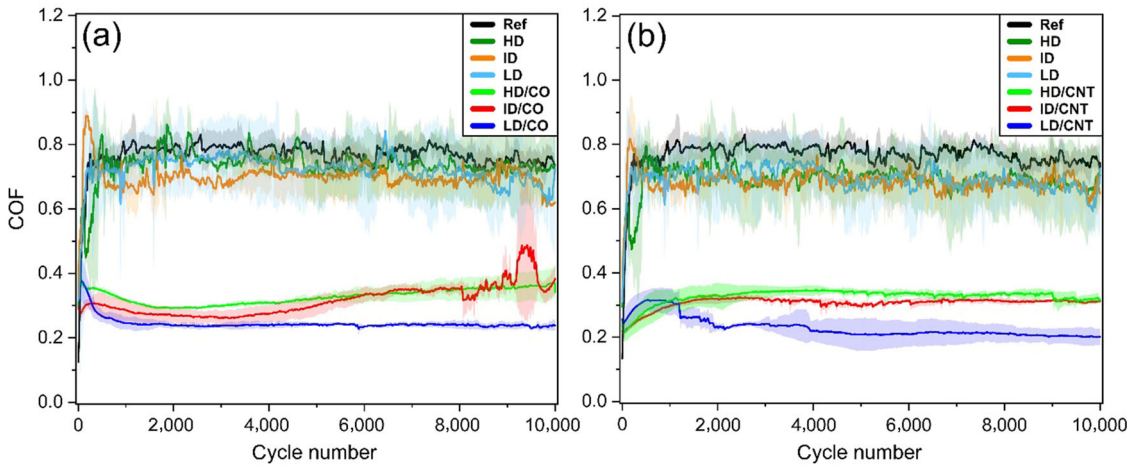

Fig. 4 Evolution of the COF of laser-patterned AISI 304 surfaces uncoated as well as coated with (a) COs or (b) CNTs.

combined with the function of the laser patterns as a reservoir. The laser pattern's structural depth greatly influences the initial COF peak value, the minimum COF, and the frictional performance towards the end of the test. The COF of HD/CO jumps to 0.40 during the first 20 cycles, followed by a steady decrease down to 0.30. After roughly 2,000 cycles, a turning point is reached, after which the COF increases steadily, reaching 0.37 after 10,000 cycles. ID/CO results in a lower peak value of 0.30 and a smaller minimum COF of 0.26. Like HD/CO, after reaching its minimum friction, the COF starts to increase again and attains a final value of just below 0.40. After 6,800 cycles, the oscillation of the COF grows stronger, resulting in a pronounced peak with a maximum COF of 0.50 after 9,400 cycles. Simultaneously, the standard deviation rises significantly.

The observed peak in the COF signal can be explained by the gradual degradation of the laser-pattern and the subsequent removal of the lubricious COs from the contact. As a result of local CO depletion, the contact area becomes inhomogeneous. This leads to a destabilization of the tribological behavior, which translates to a variable COF curve. The following return to a lower COF can be traced back to the replenishment of lubricant by tapping into a low-lying CO reservoir. For the first 5,500 cycles, ID/CO and HD/CO show near parallel COF development, with ID/CO maintaining a slightly lower COF. At the turning points, where the COF starts to increase, COs replenishment from the reservoirs begins to fade. The onset of oscillation in the case of ID/CO is a strong indicator for an at least partially unlubricated contact, leading to the degradation of the surface pattern and the formation of wear particles. The tribological performance of LD/CO differs notably from that of the deeper structures. After forming a significant peak during the first 80 cycles, the COF starts to decrease and reaches 0.24 at roughly 1,300 cycles. The COF remains constant for the following 8,700 cycles. A high reproducibility is inferred from the very low standard deviation.

Much like COs, combining laser patterns and CNT coatings leads to a significant friction reduction compared to the reference or the uncoated samples (Fig. 4(b)). ID/CNT and HD/CNT exhibit an almost identical COF development. Starting at around 0.22, their COF increases steadily to 0.31 and remains relatively constant after that. Both samples show low standard deviation during that period. For the most part, the COF of ID/CNT lies slightly below that of HD/CNT. The COF of LD/CNT rises during the initial 800 cycles. This increase is more substantial than ID/CNT or HD/CNT and could be explained by the weak-reservoir effect, meaning reservoirs are initially unable to retain the lubricant. After 1,300 cycles, there is a sudden drop from 0.30 to 0.26, followed by a gradual decrease reaching 0.20 at 4,000 cycles and remaining at that level for the final cycles. All CNT-coated/patterned surfaces can maintain a substantially lower COF than Ref and the uncoated samples over the entire test duration. Concerning the HD and ID samples, their corresponding COF developments indicate an increased lubrication lifetime of surfaces coated with CNT instead of CO, whose COF starts to increase after 2,000 and 3,000 cycles, respectively.

The shallowest CO-coated surfaces reach a COF of 0.24, whereas their CNT-coated equivalents achieve effective solid lubrication with a COF of 0.20. However, the detailed lubrication mechanisms of these particles are still being researched. In contrast to CO coatings, CNT coatings contain less coherent agglomerates alongside individual particles (Figs. 2 and 3). These particle types possess a higher range of motion and, thus, an increased ability to roll, which could explain a slightly lower COF.

An overall trend becomes apparent: the shallower the coated structure, the lower its COF, regardless of particle type. A possible explanation is related to the slopes' steepness (Figs. 2, 3(d)–3(f)) as shallow structures have a low angular slope that facilitates particle transport out of the structures and into the loaded contact area.

There is a good agreement between the COF values of the CNT-coated samples with those obtained by Schäfer et al. [22]; the latter work conducted micro tribometer tests on CNT-coated, cross-patterned stainless steel substrates with a depth of 1 and 3 μm fabricated by femtosecond laser pulses. Their results demonstrate that shallower patterned surfaces provide steady-state lubrication at a value of just under 0.20 for roughly 40,000 cycles. In contrast, the COF of the samples with higher structural depth starts to rise precipitously after a few thousand cycles and continues

until reaching that of the reference. However, all of our CNT-coated picosecond-patterned surfaces last over 10,000 cycles and more. While lubricating at maximum capacity, the coated surfaces with the deeper pattern (3 μm) showed slightly lower COF values than the shallower samples (1 μm) in contrast to our findings. Nonetheless, the samples were subject to a different type of tribological stress as Schäfer et al. measured in rotational mode with a higher load (1 N) [22].

Figures 2 and 3(f) show that before the tribological tests, the deep structures were not completely filled with particles during EPD as the shallower ones have. Nevertheless, the deeper patterns also demonstrated an effective COF reduction over significant periods during the tribological tests, albeit not as effective as the shallower patterns. Therefore, FIB cross-sections were prepared from inside the wear track of the HD samples after the initial 10 cycles of the friction test (Fig. 5). As seen, the particles get pressed into the structures from where they supply the contact with continuous lubrication as demonstrated by the results of the tribological tests. Due to their higher packing density, the CNTs can fill the structures more densely than the COs (Figs. 5(a) and 5(b)) which also explains the previously observed weak-reservoir effect. Large, coherent chunks of amorphous carbon and/or entangled CNTs are removed at once from the top of the reservoir bequeathing a superficial particle depletion which results in a temporary COF increase. Once the lower lubricant-filled regions of the reservoir get in contact, lubricant supply resumes and the COF increase is reversed. This effect is more likely to occur on shallow structures as their flat flanks facilitate lubricant removal and their filling ratio is higher compared to that of deep structures (Figs. 2 and 3) and, therefore, less compressible. In deep structures on the other hand, counter body pressure during tribological stress leads to a filling of existing voids and the particles are pressed further down the structure, preventing the above-mentioned removal mechanism. Additionally, the CNTs' known ability for mechanical restitution after compression in tribological contacts [23] combined with their large aspect ratio facilitates particle feed into the contact area, which could be why a weak-reservoir effect of similar magnitude is not observed for COs.

Furthermore, the CNT coatings in Fig. 5 remain largely intact after the initial cycles while the majority of the CO coating is removed. This can be explained by the particles' morphology. As the CNTs within the coating are highly entangled, they form a cohesive unit which is significantly more difficult to remove than an accumulation of large CO agglomerates.

3.3 Wear track and chemical analysis

3.3.1 HD pattern

To further understand the mechanisms responsible for the observed friction reduction, the occurred wear tracks were analyzed. SEM was used for identifying the primary wear mechanisms on representative wear tracks of each tested surface. At a higher resolution (Fig. 6(a)), the line pattern of the uncoated HD sample

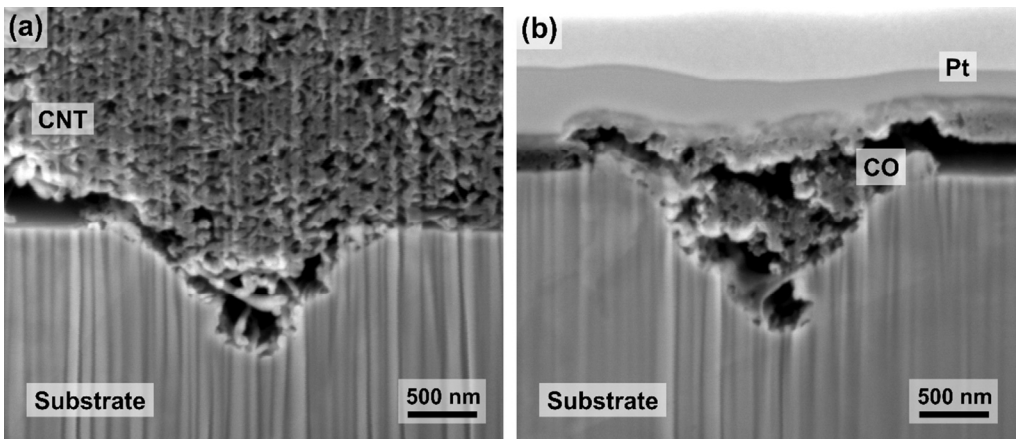

Fig. 5 SEM images showing cross-sections of (a) CNT-coated and (b) CO-coated picosecond-laser processed AISI 304 steel surfaces after 10 tribological cycles (HD sample).

has been completely worn off during the friction tests. Particularly in unlubricated tribological contacts, different wear mechanisms act simultaneously. In this case, sharp horizontal grooves are visible, stemming from both abrasive oxide particles formed during the tribo-test, and the asperities of the counter body. The most dominant wear mechanism, however, is adhesion which is caused by solid-state welding. Adhesion marks are visible in the wear tracks of all uncoated samples in the form of dark spots.

EDS was used to acquire elemental maps to get a better understanding of the tribo-chemical reactions during friction testing. The large bright green areas inside the wear track of the uncoated HD sample depicted in Fig. 6(b) indicate extensive oxidation and severe tribo-chemical wear, which conforms perfectly with the high COF value measured during tribological testing. It also shows that the material pile-up at the right edge of the wear track consists mainly of oxide particles.

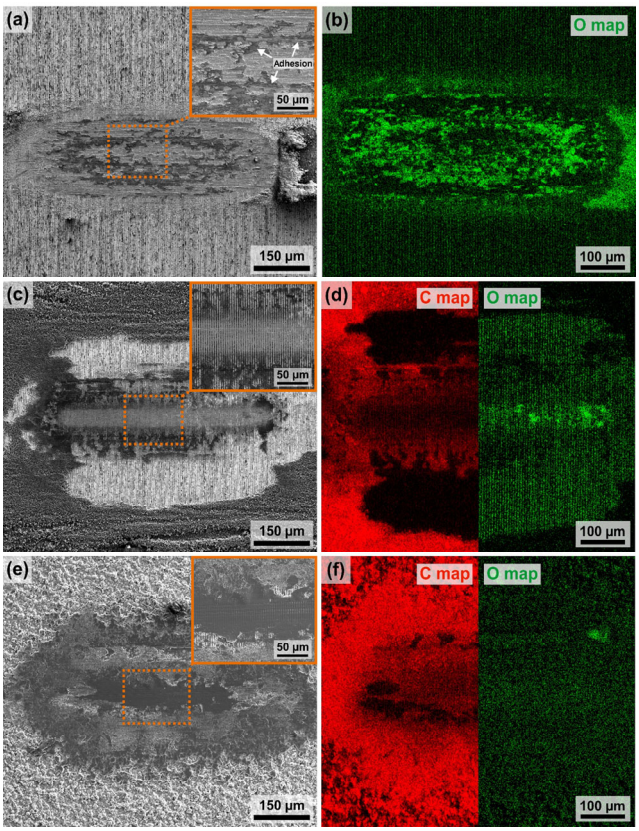

Fig. 6 SEM images of (a) uncoated, (c) CO-coated, and (e) CNT-coated wear tracks on the high depth patterns after friction testing with their corresponding EDS maps of carbon and oxygen (b, d, f).

Figure 6(c) provides an overview of the wear track on the CO-coated HD surface. In the magnified image, the line pattern in the center of the wear track is still clearly recognizable, despite showing a substantial degree of degradation. Particularly in areas on the left side of the wear track, where the pattern is better preserved, vertical dark lines are visible. Those lines represent carbon reservoirs in the remnants of the pattern's recessions. However, most of the coating in and around the wear track was removed during the friction test, confirmed by the carbon map shown in Fig. 6(d), as no carbon signals were detected outside of the wear track.

The remaining carbon reservoirs are also verified by vertical red lines inside the wear track. In the oxygen map (Fig. 6(d)), the wear track appears in a slightly brighter green compared to the surrounding substrate. Especially the right part contains areas of bright green, indicating mild oxidative wear. Simultaneously, the complete carbon map (Fig. 7) shows a near-complete absence of carbon in that particular area, leading to a higher mechanical impact on the substrate, resulting in faster oxidation. The measured COF of this sample, which is 0.37 after 10,000 cycles, correlates well with the observed wear behavior. The COF is well above the threshold of 0.20, which is considered effective lubrication according to Aouadi et al. [45], with no signs of wear. The measured COF is far below that of the patterned/uncoated sample, where severe wear and oxidation were observed (Fig. 6(b)).

Figure 6(e) shows the CNT-coated wear track of the HD sample after tribological testing, which, in

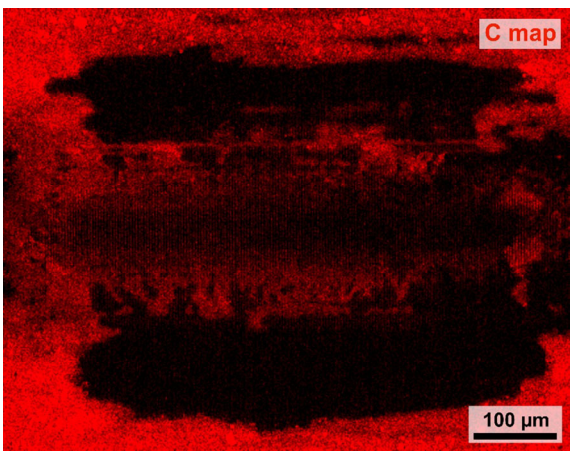

Fig. 7 Elemental carbon map of the CO-coated wear track on the HD surface after friction testing.

contrast to the CO-coated surface, is still largely covered by the coating. This can be attributed to a stronger cohesion of the CNT-coating resulting from the particles' entanglement. Those particles inside the wear track, which were in contact with the counter body, appear darker than the surrounding CNT-coating, most likely because of compression. Further magnification of the wear track shows that after 10,000 cycles, the line pattern underneath the coating remains fully intact. The carbon map (Fig. 6(f)) reveals that carbon has been detected throughout the wear track in the same locations as the compressed portions of carbon (Fig. 6(e)). At the same time, there is no strong oxygen signal inside the wear track (Fig. 6(f)); hence no significant oxidation has occurred.

3.3.2 *ID pattern*

Like the HD sample, the uncoated wear track of the ID sample depicted in Fig. 8(a) shows extensive wear due to which the line pattern was removed entirely.

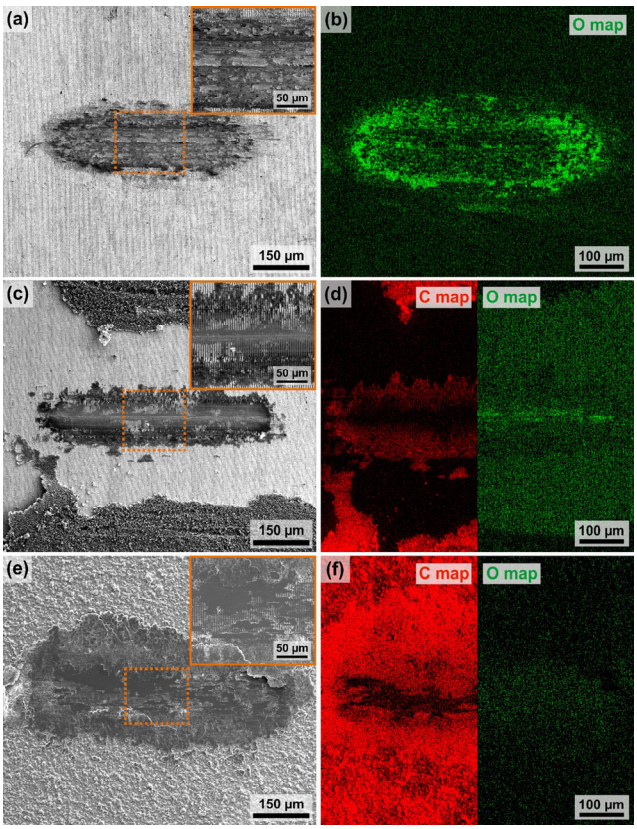

Fig. 8 SEM images of (a) uncoated, (c) CO-coated, and (e) CNT-coated wear tracks on the intermediate depth patterns after friction testing with their corresponding EDS maps of carbon and oxygen (b, d, f).

Particularly at higher resolution (Fig. 8(a)), adhesion is clearly identifiable as the dominant wear mechanism. As to be expected, the oxygen map (Fig. 8(b)) shows severe tribo-induced oxidation. However, in this case, there was no pile-up of oxide particles at the end of the wear track.

Figure 8(c) shows the wear track of the CO-coated and laser-patterned ID substrate, and as observed previously for the sample with the highest structural depth (Fig. 6(c)), most of the surrounding CO-coating was removed. Abrasive wear occurring in the center of the wear track, where the contact pressure was highest, induced a pronounced groove in sliding direction, stretching over the wear track's entire length. Apart from the groove, the line pattern in the contact area is still intact. The carbon map in Fig. 8(d) reveals a complete absence of carbon in the groove. Outside the groove, carbon is detected in the topographical minima of the pattern in the same locations as the dark areas in Fig. 8(c). The lack of lubricious carbon nanoparticles results in oxidation, as depicted in the oxygen map (Fig. 8(d)). Mild oxidation occurs along the groove, comparable to that of the HD pattern (Fig. 6(d)). The comparable wear behavior of the CO-coated samples with high and intermediate structural depth is in strong agreement with their final COF values, which are also close to identical.

Figure 8(e) shows the CNT-coated wear track of the ID sample. Despite the considerable sliding duration, large areas of the wear track remain CNT-covered, which is confirmed by the carbon map (Fig. 8(f)). Furthermore, a pristine laser pattern is recognizable underneath the coating in Fig. 8(e). At the same time, no oxidation has occurred according to the oxygen map (Fig. 8(f)).

3.3.3 *LD pattern*

Following the previous uncoated samples' wear behavior, the sample's wear track with the lowest structural depth shown in Fig. 9(a) is severely worn out, with abrasion and adhesion being the dominant wear mechanisms. Once again, the oxygen map in (Fig. 9(b)) confirms strong oxidation. Despite varying fluences and, therefore, different structural depths, all the uncoated wear tracks' wear and oxidation behavior is very similar, which stands in good agreement with their respective friction behavior.

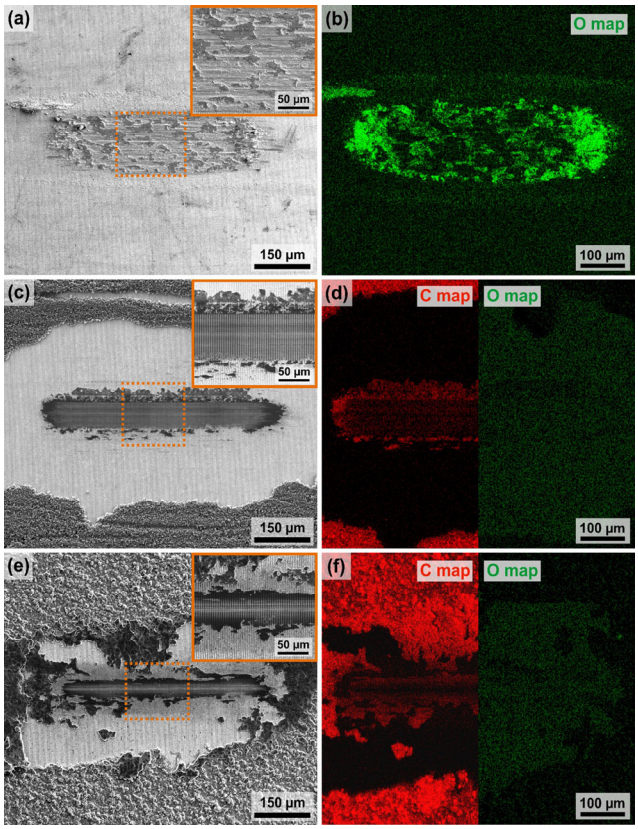

Fig. 9 SEM images of (a) uncoated, (c) CO-coated, and (e) CNT-coated wear tracks on the low depth patterns after friction testing, with their corresponding EDS maps of carbon and oxygen (b, d, f).

Figure 9(c) shows the CO-coated wear track of the surface, which was laser-processed at the lowest fluence, resulting in the lowest depth. In contrast to CNT, the removal of CO coatings directly surrounding the wear track seems to be characteristic and is attributed to a weak coating-substrate adhesion. As a result of large agglomerates' formation, COs are removed in large flakes upon contact with the counter body. Nevertheless, the dark vertical lines within the wear track depicted in Fig. 9(c), represent homogeneously filled structures in a near-pristine surface pattern. EDS mapping (Fig. 9(d)) confirms carbon in the structures, while no oxidation was detected (Fig. 9(d)). Overall, the average pattern on CO-coated surfaces with shallow structural depth is well sustained. In contrast to deeper patterns, no significant abrasion is observed. Fittingly, tribological testing performed on the shallowest CO-coated patterns shows the lowest COF.

As observed in the previous wear tracks of CNT-coated samples, the wear track on the shallowest surface pattern in Fig. 9(e) also shows large dark areas of compressed carbon nanoparticles around the wear track. The fact that parts of the surrounding CNT-coating are compressed implies direct contact with the counter body. This translates to an increased load distribution on the surface, thus reducing the load on the wear track. Moreover, the elastic restitution inherent to CNT particles exerts a counter pressure on the alumina ball, therefore, further relieving load from the wear track. Generally, the coating surrounding the CO-coated wear tracks is largely removed, which might contribute to the superior lubrication properties of CNT coatings compared to CO coatings.

The laser pattern on the LD surface depicted in Fig. 9(e) is mainly intact with particle filled structures. The elemental map in Fig. 9(f) confirms the carbon in said structures. This concludes that small amounts of CNT are sufficient to lubricate the contact and ensure a low COF effectively. No significant oxidation has occurred despite the diminished carbon content in the wear track's centerline (Fig. 9(f)). Also, no oxidation was detected for the ID and HD patterns, even though the COF was about 0.30, while the threshold of effective lubrication is 0.20. This can be explained by individual particles dragged from the reservoirs and/or extensive coating residuals on the wear tracks, thereby effectively preventing direct contact between the substrate surface and counter body and, thus, oxidation. After tribological testing, the wear tracks on the HD and ID structures are still largely covered by coherent patches of CNT-coating (Figs. 6 and 8(e)), with the corresponding patterns fully intact, suggesting a significantly longer lubrication lifetime. As previously mentioned, the CNT-coated LD patterns show the lowest COF values during friction testing despite completely lacking said patches, which cover the underlying pattern. The improved lubricity could be due to a direct supply of individual particles or small agglomerates from the reservoirs, which possess a relatively high degree of mobility and flexibility opposed to stationary coherent patches on top of the pattern. Irrespective of structural depth, all CNT-coated line patterns are well preserved after 10,000 testing cycles with little to no signs of degradation.

3.4 Microstructural characterization

We used TEM to investigate the impact of DLIP processing with laser pulses in the picosecond range on the underlying microstructure of AISI 304 stainless steel. Figures 10(a)–10(c) show cross-sections of the near-surface microstructure of the uncoated reference samples. Independent of structural depth, no significant differences can be observed between the original microstructure of the lower regions and the superficial microstructure. This illustrates that with the parameters used, the microstructure remains unaffected by picosecond DLIP processing at the displayed scale. However, microstructural changes may still occur on a smaller scale not visible in the existing TEM images.

Bieda et al. [46] simulated the thermal effect of picosecond DLIP on stainless steel (iron), among other metals, based on the two-temperature model. The resulting data reveal that thermal absorption depth (also referred to as thermal diffusion length) exceeded 250 nm at 425 ps. A reduced pulse duration to 35 ps significantly reduced thermal absorption depth to roughly 80 nm. A duration of 10 ps is the threshold to the ultrashort pulse regime below which the interaction is dominated by cold ablation. Based on Bieda's calculations, the thermal absorption depth further decreases to 45 nm at the pulse duration of 12 ps used in this study, as the ablative characteristics become increasingly non-thermal. Moreover, Artyukov et al. [47] conducted a study on electron/lattice

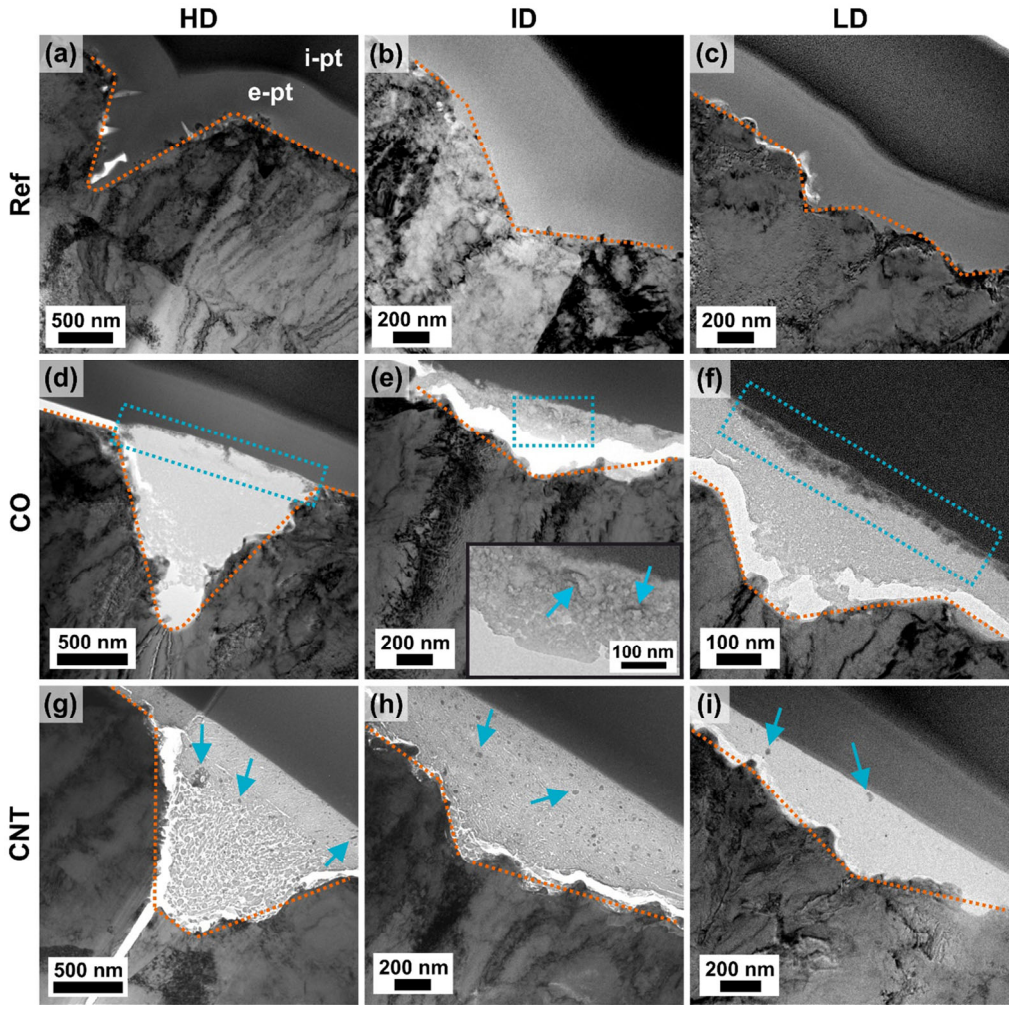

Fig. 10 Near-surface cross-sectional TEM images of (a–c) uncoated reference, (d–f) CO- and (g–i) CNT-coated structures with different structural depths. Both CO- and CNT-coated surfaces have been exposed to 10,000 cycles of tribological testing. The dotted orange lines draw the course of the surface. The blue arrows and blue dotted areas mark the areas where wear particles accumulate in the CO and CNT tribofilm, respectively.

relaxation phenomena of iron exposed to sub- and picosecond laser pulses (0.3–3.6 ps). Particularly at higher pulse durations, the obtained data suggest that ultrafast evaporative cooling is the dominant surface process following ablation, suggesting a low thermal impact on the underlying microstructure. Considering the results of both studies, it is viable to assume that thermally affected areas remain small and highly localized at the edges of the grooves. Thus, a large-scale alteration of the microstructure remains absent. REF was not exposed to friction testing and no microstructural changes can be observed

TEM was further used to examine whether the applied tribological load affects the underlying microstructure of the CO- (Figs. 10(d)–10(f)) and CNT-coated (Figs. 10(g)–10(i)) surfaces as well as to image the formed tribofilm. In both cases, microstructural damage such as deformation remains completely absent, regardless of structural depth and, thus, topography. As illustrated in Figs. 10(g), the CNTs at the bottom of the pattern's recession remain relatively pristine. However, continuous mechanical degradation of the CNTs close to the contact area induces the formation of a carbonaceous tribofilm that contains a significant share of at least partially amorphized CNTs, along with wear particles. Regarding the CO-coating, no structural changes can be observed at this scale. The coating types differ in the way they store resulting wear particles. As marked by the dotted blue lines in Figs. 10(d) and 10(f), wear particles seem to accumulate preferably directly at the tribofilm/Pt interface in CO-derived tribofilms. In CNT-derived tribofilms (Figs. 10(g)–10(i)) by contrast, wear particles are distributed randomly (marked by blue arrows).

Further, Fig. 11 suggests the formation of covalent bonds between CNTs and the substrate surface (marked by the orange circle), which mechanically anchor the particles to the surface, effectively keeping them in contact and, thus, increasing overall lubricity. The bond formation seems to occur at a local peak where the contact pressure is significantly increased by which a corresponding bonding reaction is made possible.

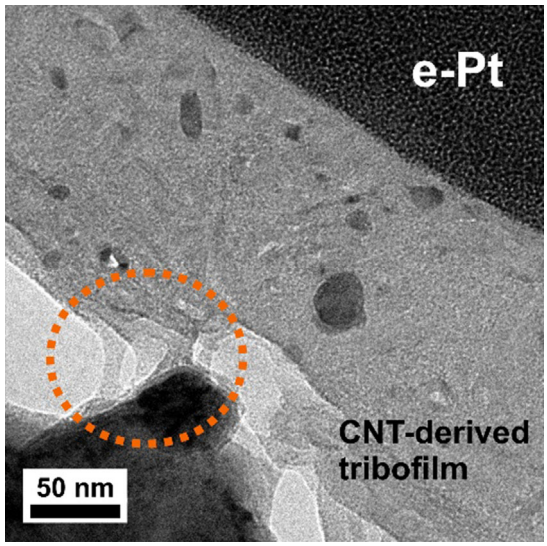

Fig. 11 Cross-sectional transmission electron micrograph of the CNT/substrate (LD) interface after friction testing.

4 Conclusions

We present a comprehensive study on the influence of the structural depth of line patterns on AISI 304 stainless steel coated with either carbon nanotubes (CNTs) or carbon onions (COs), on their solid lubricity.

Coating the surfaces with CNTs or COs always leads to a significant coefficient of friction (COF) reduction compared to their uncoated equivalent or the non-patterned reference, achieving a COF reduction factor between 2 and 4. During the studied contact scenario at low humidity and otherwise ambient conditions, CNTs exhibit superior lubricity compared to COs. Regarding the influence of the structural depth, a trend emerges from the results of the tribological experiments: the shallower the structure, the lower the COF of the respectively coated surface. Despite slightly different surface topographies and experimental conditions, the obtained results are in good agreement with those of a closely related work by Schäfer et al. [22]. The observed phenomenon could be attributed to the facilitation of particle supply from the reservoirs into the contact as slope steepness decreases. This allows for an adequate amount of lubricant in the contact areas leading to a lower COF. There is a distinction between the influence of structural depth and the steepness of the flanks. However, in this work, the structural depth of the pattern and flank steepness are inherently connected due to the material removal mechanism caused by laser pulses in the picosecond range. Wear track analysis after tribological testing has shown that the line patterns in CNT-coated wear tracks were largely preserved without

any surface oxidation being detected. In contrast, the intermediate and deep CO-coated structures exhibit significant wear along with mild surface oxidation as shown by energy-dispersive X-ray spectroscopy (EDS) mapping, which is fittingly reflected by their COF development. A possible explanation for the superior friction and wear-reducing properties of CNTs is the high aspect ratio, which enables the particles to be dragged directly into the contact region more easily. In addition, cross-sectional transmission electron microscopy (TEM) characterization has shown the underlying microstructure of the AISI 304 substrate to remain unaltered by both picosecond direct laser interference patterning (DLIP) processing and the applied tribological load.

The results obtained in this study demonstrate the importance of optimizing the surface design to maximize the lubrication performance of CNT/CO-coated and laser-patterned stainless-steel surfaces.

Acknowledgements

T. MacLucas and S. Suarez wish to kindly acknowledge financial support by the Deutsche Forschungsgemeinschaft (DFG, German Research Foundation) within the project MU 959/47-1. Furthermore, the authors gratefully acknowledge funding in the ZuMat project, supported by the State of Saarland from the European Regional Development Fund (Europäischer Fonds für Regionale Entwicklung, EFRE). P. Grützmacher and C. Gachot would like to thank the Government of Lower Austria (WST3) for financially supporting the endowed professorship tribology at the TU Wien. V. Presser thanks Eduard Arzt (INM) for his continuing support.

References

[1] Rosenkranz A, Reinert L, Gachot C, Mücklich F. Alignment and wear debris effects between laser-patterned steel surfaces under dry sliding conditions. *Wear* **318**(1–2): 49–61 (2014)

[2] Gachot C, Rosenkranz A, Reinert L, Ramos-Moore E, Souza N, Müser M H, Mücklich F. Dry friction between laser-patterned surfaces: Role of alignment, structural wavelength and surface chemistry. *Tribol Lett* **49**: 193–202 (2013)

[3] Rosenkranz A, Heib T, Gachot C, Mücklich F. Oil film lifetime and wear particle analysis of laser-patterned stainless steel surfaces. *Wear* **334–335**: 1–12 (2015)

[4] Etsion I. State of the art in laser surface texturing. *J Tribol* **127**: 248–253 (2005)

[5] Chilamakuri S K, Bhushan B. Optimization of asperities for laser-textured magnetic disk surfaces. *Tribol Trans* **40**(2): 303–311 (1997)

[6] Song Y, Premachandran Nair R, Zou M, Wang Y A. Adhesion and friction properties of micro/nano-engineered superhydrophobic/hydrophobic surfaces. *Thin Solid Films* **518**(14): 3801–3807 (2010)

[7] Mücklich F, Lasagni A, Daniel C. Laser interference metallurgy—Periodic surface patterning and formation of intermetallics. *Intermetallics* **13**(3–4): 437–442 (2005)

[8] Mücklich F, Lasagni A, Daniel C. Laser interference metallurgy—Using interference as a tool for micro/nano structuring. *Int J Mater Res* **97**(10): 1337–1344 (2006)

[9] Scharf TW, Prasad S V. Solid lubricants: A review. *J Mater Sci* **48**: 511–531 (2013)

[10] Rosenkranz A, Grützmacher P G, Espinoza R, Fuenzalida V M, Blanco E, Escalona N, Gracia F J, Villarroel R, Guo L C, Kang R Y, Mucklich F, Suarez S, Zhang Z Y. Multi-layer $Ti_3C_2T_x$-nanoparticles (MXenes) as solid lubricants—Role of surface terminations and intercalated water. *Appl Surf Sci* **494**: 13–21 (2019)

[11] Reinert L, Suárez S, Rosenkranz A. Tribo-mechanisms of carbon nanotubes: Friction and wear behavior of CNT-reinforced nickel matrix composites and CNT-coated bulk nickel. *Lubricants* **4**(2): 11 (2016)

[12] Reinert L, Green I, Gimmler S, Lechthaler B, Mücklich F, Suàrez S. Tribological behavior of self-lubricating carbon nanoparticle reinforced metal matrix composites. *Wear* **408–409**: 72–85 (2018)

[13] Scharf T W, Neira A, Hwang J Y, Tiley J, Banerjee R. Self-lubricating carbon nanotube reinforced nickel matrix composites. *J Appl Phys* **106**: 013508 (2009)

[14] Kim K T, Cha S, Hong S H. Hardness and wear resistance of carbon nanotube reinforced Cu matrix nanocomposites. *Mater Sci Eng A* **449–451**: 46–50 (2007)

[15] Suárez S, Rosenkranz A, Gachot C, Mücklich F. Enhanced tribological properties of MWCNT/Ni bulk composites—Influence of processing on friction and wear behaviour. *Carbon* **66**: 164–171 (2014)

[16] Tan J, Yu T, Xu B, Yao Q. Microstructure and wear resistance of nickel-carbon nanotube composite coating from brush plating technique. *Tribol Lett* **21**: 107–111 (2006)

[17] Guiderdoni C, Estournès C, Peigney A, Weibel A, Turq V, Laurent C. The preparation of double-walled carbon nanotube/Cu composites by spark plasma sintering, and their hardness and friction properties. *Carbon* **49**: 4535–4543 (2011)

[18] Reinert L, Varenberg M, Mücklich F, Suárez S. Dry friction and wear of self-lubricating carbon-nanotube-containing surfaces. *Wear* **406–407**: 33–42 (2018)

[19] Thomas B J C, Boccaccini A R, Shaffer M S P. Multi-walled carbon nanotube coatings using electrophoretic deposition (EPD). *J Am Ceram Soc* **88**(4): 980–982 (2005)

[20] MacLucas T, Suarez S. On the solid lubricity of electrophoretically deposited carbon nanohorn coatings. *Lubricants* **7**(8): 62 (2019)

[21] Xu J, Chen X, Grützmacher P, Rosenkranz A, Li J, Jin J, Zhang C H, Luo J B. Tribochemical behaviors of onion-like carbon films as high-performance solid lubricants with variable interfacial nanostructures. *ACS Appl Mater Interfaces* **11**: 25535–25546 (2019)

[22] Schäfer C, Reinert L, MacLucas T, Grützmacher P, Merz R, Mücklich F, Suarez S. Influence of surface design on the solid lubricity of carbon nanotubes-coated steel surfaces. *Tribol Lett* **66**: 89 (2018)

[23] Reinert L, Lasserre F, Gachot C, Grützmacher P, MacLucas T, Souza N, Mucklich F, Suarez S. Long-lasting solid lubrication by CNT-coated patterned surfaces. *Sci Rep* **7**: 42873 (2017)

[24] MacLucas T, Schütz S, Suarez S, Mücklich F. Surface protection of austenitic steels by carbon nanotube coatings. *Surf Topogr Metrol Prop* **6**: 014005 (2018)

[25] Reinert L, Schütz S, Suárez S, Mücklich F. Influence of surface roughness on the lubrication effect of carbon nanoparticle-coated steel surfaces. *Tribol Lett* **66**: 45 (2018)

[26] Hirata A, Igarashi M, Kaito T. Study on solid lubricant properties of carbon onions produced by heat treatment of diamond clusters or particles. *Tribol Int* **37**(11–12): 899–905 (2004)

[27] Hirata A, Yoshioka N. Sliding friction properties of carbon nanotube coatings deposited by microwave plasma chemical vapor deposition. *Tribol Int* **37**(11–12): 893–898 (2004)

[28] Dickrell P L, Pal S K, Bourne G R, Muratore C, Voevodin A A, Ajayan P M, Schadler L S, Sawyer W G. Tunable friction behavior of oriented carbon nanotube films. *Tribol Lett* **24**: 85–90 (2006)

[29] Miyoshi K, Street K W, Vander Wal R L, Andrews R, Sayir A. Solid lubrication by multi-walled carbon nanotubes in air and in vacuum. *Tribol Lett* **19**: 191–201 (2005)

[30] Zhang R, Ning Z, Zhang Y, Zheng Q, Chen Q, Xie H, Zhang Q, Qian W Z, Wei F. Superlubricity in centimetres-long double-walled carbon nanotubes under ambient conditions. *Nat Nanotechnol* **8**: 912–916 (2013)

[31] Berman D, Narayanan B, Cherukara M J, Sankaranarayanan S K R S, Erdemir A, Zinovev A, Sumant A V. Operando tribochemical formation of onion-like-carbon leads to macroscale superlubricity. *Nat Commun* **9**: 1164 (2018)

[32] Berman D, Deshmukh S A, Sankaranarayanan S K R S, Erdemir A, Sumant A V. Macroscale superlubricity enabled by graphene nanoscroll formation. *Science* **348**(6239): 1118–1122 (2015)

[33] Gong Z, Bai C, Qiang L, Gao K, Zhang J, Zhang B. Onion-like carbon films endow macro-scale superlubricity. *Diam Relat Mater* **87**: 172–176 (2018)

[34] Yu M F, Lourie O, Dyer M J, Moloni K, Kelly T F, Ruoff R S. Strength and breaking mechanism of multi-walled carbon nanotubes under tensile load. *Science* **287**(5453): 637–640 (2000)

[35] Wong E W, Sheehan P E, Lieber C M. Nanobeam mechanics: Elasticity, strength, and toughness of nanorods and nanotubes. *Science* **277**(5334): 1971–1975 (1997)

[36] Salvetat J P, Bonard J M, Thomson N B, Kulik A J, Forró L, Benoit W, Zuppiroli L. Mechanical properties of carbon nanotubes. *Appl Phys A* **69**: 255–260 (1999)

[37] Meyers M A, Mishra A, Benson D J. Mechanical properties of nanocrystalline materials. *Prog Mater Sci* **51**(4): 427–556 (2006)

[38] Rosenkranz A, Costa H L, Baykara M Z, Martini A. Synergetic effects of surface texturing and solid lubricants to tailor friction and wear—A review. *Tribol Int* **155**: 106792 (2021)

[39] Thomas B J C, Shaffer M S P, Freeman S, Koopman M, Chawla K K, Boccaccini A R. Electrophoretic deposition of carbon nanotubes on metallic surfaces. *Key Eng Mater* **314**: 141–146 (2006)

[40] Boccaccini A R, Cho J, Roether J A, Thomas B J C, Jane Minay E, Shaffer M S P. Electrophoretic deposition of carbon nanotubes. *Carbon* **44**(15): 3149–3160 (2006)

[41] Wu Z S, Pei S, Ren W, Tang D, Gao L, Liu B, Li F, Liu C, Chen H M. Field emission of single-layer graphene films prepared by electrophoretic deposition. *Adv Mater* **21**(17): 1756–1760 (2009)

[42] Zeiger M, Jäckel N, Aslan M, Weingarth D, Presser V. Understanding structure and porosity of nanodiamond-derived carbon onions. *Carbon* **84**: 584–598 (2015)

[43] Ayache J, Beaunier L, Boumendil J, Ehret G, Laub D. *Sample preparation handbook for transmission electron microscopy: Techniques*. Springer Science & Business Media, 2010.

[44] Blau P J. On the nature of running-in. *Tribol Int* **38**(11–12): 1007–1012 (2005)

[45] Aouadi S M, Gao H, Martini A, Scharf T W, Muratore C. Lubricious oxide coatings for extreme temperature applications: A review. *Surf Coat Technol* **257**: 266–277 (2014)

[46] Bieda M, Siebold M, Lasagni A F. Fabrication of sub-micron surface structures on copper, stainless steel and titanium using picosecond laser interference patterning. *Appl Surf Sci* **387**: 175–182 (2016)

[47] Artyukov I A, Zayarniy D A, Ionin A A, Kudryashov S I, Makarov S V, Saltuganov P N. Relaxation phenomena in electronic and lattice subsystems on iron surface during its ablation by ultrashort laser pulses. *JETP Lett* **99**: 51–55 (2014)

Timothy MACLUCAS. He received his bachelor's degree in materials and process engineering in 2014 from Zurich University of Applied Sciences. In 2016, he obtained a joint master's degree in advanced materials science and engineering from Saarland University and Luleå University of Technology. Currently, he is working as a doctoral researcher at the Chair of Functional Materials at Saarland University. His research fields include electrophoretic deposition of carbon nanoparticles and tribological properties of carbon nanoparticle coatings on surface-structured metals.

Carsten GACHOT. He received his Ph.D. from the Saarland University in Germany in 2012 where he studied the effects of laser interference patterning on the microstructure and topography of metallic surfaces with a focus on tribological applications under Prof. Frank Mücklich and Prof. Martin H. Müser. For this work, he was awarded by the European Honda initiation grant in 2011. Prof. Gachot was academic visitor at the tribology group at Imperial College London and is currently the head of the tribology research group at Vienna University of Technology. Additionally, he is a visiting professor at Pontifical Catholic University in Santiago de Chile and chief editor of the peer reviewed journal *Industrial Lubrication and Tribology* of the Emerald Publishing Group Leeds UK.